SUPPLEMENTARY INFORMATION:

Triplet State Formation and Quenching Dynamics of 2-Mercaptobenzothiazole in Solution

Daisuke Koyama and Andrew J. Orr-Ewing

School of Chemistry, University of Bristol, Cantock's Close, Bristol BS8 1TS, UK

ADDITIONAL EXPERIMENTAL AND COMPUTATIONAL DETAILS

Transient electronic absorption spectroscopy (TEAS) and transient vibrational absorption spectroscopy (TVAS) of thioxanthone (97%, Sigma Aldrich, used as received) were performed using the same methods as described in the main article, except for the use of a 370 nm UV pump laser wavelength. The concentration of thioxanthone in methanol or styrene solution was adjusted to give an optical density of ~0.5 OD at 370 nm (2.4 mM for TEAS and 9.2 mM for TVAS experiments).

Infrared frequencies for triplet styrene and triplet adducts mentioned in the main article were calculated using the Gaussian 09 package,[1] at the B3LYP/6-311++G(3df,3pd) level of theory.[2, 3] Calculations of electronic absorption spectra of the triplet styrene, β_{CS}-^{3}[MBT-St] (or simply ^{3}[MBT-St] in the main article) and α_{CS}-^{3}[MBT-St] used time-dependent density functional theory (TDDFT) methods with the 6-311++G(3df,3pd) basis set. Transition states for addition reactions were characterized using the CAM-B3LYP-D3 density functional,[4, 5] and the 6-311+G(d,p) basis set, because valid transition states could not be found with the B3LYP method.[6] The identification of the transition states was confirmed by subsequent intrinsic reaction coordinate (IRC) calculations, with the exception of the transition state connecting the

β_{CS}-^{3}[MBT-St] and a non-dissociated ^{3}[MBT·St] complex which has MBT (S_0) and St (T_1) character (denoted as TS ^{3}[MBT·St] complex in Figure S9). The TS ^{3}[MBT·St] complex could not be found with general transition state search methods. Instead, a potential energy of the TS ^{3}[MBT·St] complex was estimated from the maximum energy found during a relaxed potential energy scan along a reaction pathway from the β_{CS}-^{3}[MBT-St] to the ^{3}[MBT·St] complex.

Potential energy curves (PECs), equilibrium excited state geometries and infrared frequencies for the MBT thione form, and vertical excitation energies and transition dipole moments of the MBT thiol form were calculated using the Molpro package.[7] The PECs of the MBT thione form and the vertical excitation energies of the MBT thiol tautomer were calculated using the state averaged complete active space self-consistent field (SA-CASSCF) method with the aug-cc-pVTZ basis set. The geometries of the thione form at each C=S bond distance and out-of-plane C=S and N-H angles, and the equilibrium geometry of the MBT thiol form were optimized with the Gaussian 09 package using Møller-Plesset second-order perturbation theory (MP2) and the aug-cc-pVTZ level of theory.[8, 9] During the geometry optimizations involving changes of out-of-plane angles, the remaining atoms were constrained to stay in a plane.

Complete active space with second-order perturbation theory (CASPT2) energies were calculated using the SA-CASSCF result as a reference wavefunction. An imaginary level shift of 0.4 a.u. was used for all of the CASPT2 calculations to avoid intruder state problems. The PEC calculations included eight electrons in seven active orbitals (8/7) comprising the non-bonding thione S orbital, the three π and the three corresponding π^* orbitals. These orbitals correspond to the molecular orbitals numbered 40 - 46 illustrated in Figure S1. The vertical excitation energies of the MBT thiol form were calculated including six electrons in six active orbitals (6/6). These active spaces consist of three π and the three corresponding π^* orbitals (Figure S1). Geometry optimizations and fundamental infrared transition

frequency calculations for the MBT S_1, T_1 and T_2 states, as well as the S_0 state, were performed at the CASPT2 (8/7)/cc-pVTZ and 6-311+G(d,p) level of theory (i.e., with a smaller basis set than used for the PEC calculations) using the CASPT2 gradients with the SA-CASSCF results.

1. Molecular Orbitals of MBT Thione and Thiol Forms

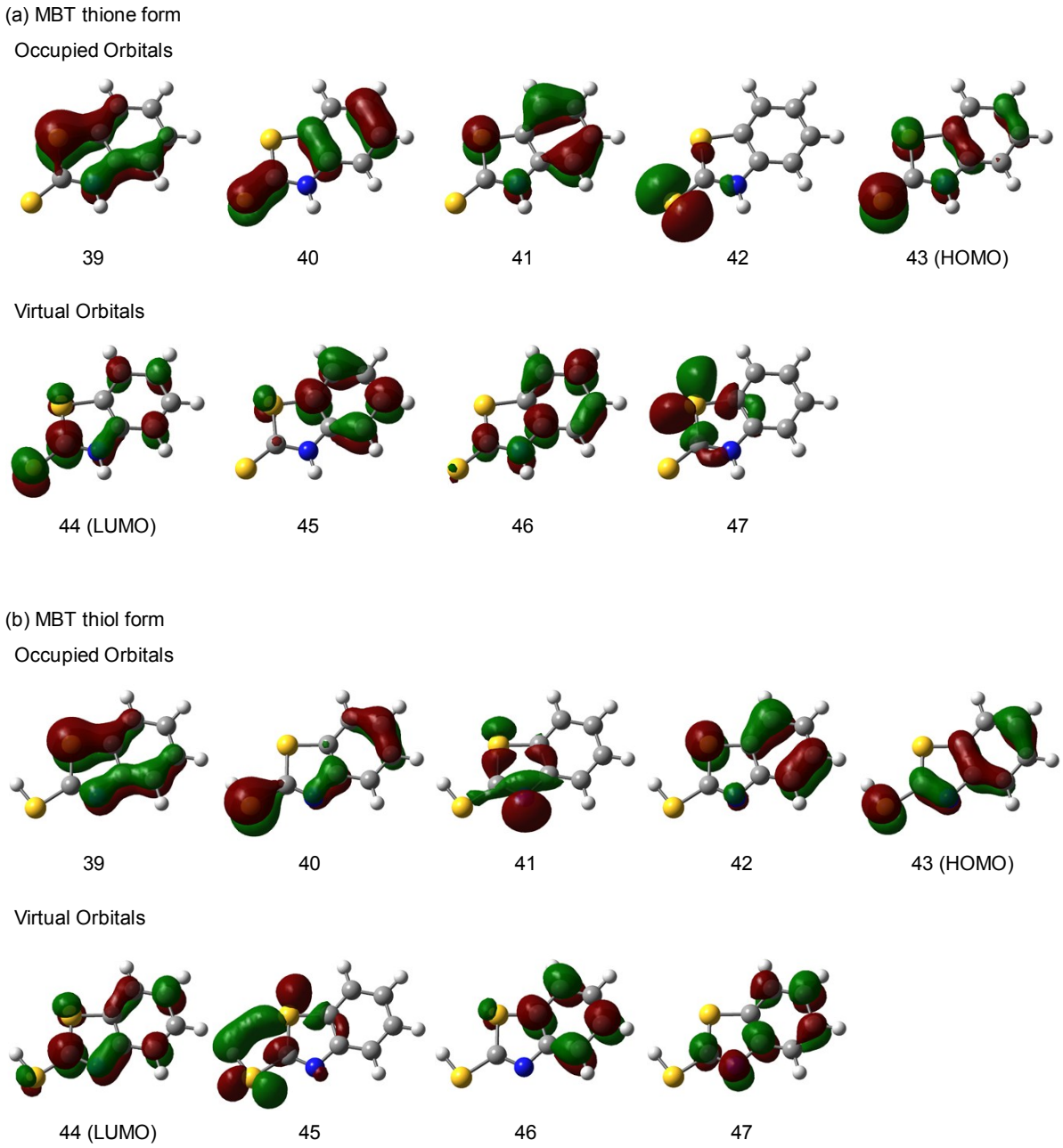

Figure S1: Molecular Orbitals of MBT (a) thione and (b) thiol tautomers at the ground state equilibrium geometry. For the thione form, the MOs numbered 40 - 46 were included in the CASSCF calculations employed in the work presented in the main article, whereas the calculation for the thiol form included MOs numbered 40, 42 - 45 and 46 - 47.

2. Vertical Excitation Energies and Transition Dipole Moments for the MBT Thiol Form

Table S1: Calculated vertical excitation energies and transition dipole moments for the thiol form of MBT, obtained at the CASPT2//CASSCF (6/6)/aug-cc-pVTZ level of theory.

Transition	Excitation energy / eV	Excitation wavelength / nm	Transition dipole moment / Debye
S_1 ($\pi\pi^*$)	4.15	299	0.3
S_2 ($\pi\pi^*$)	4.91	253	4.7

3. Steady State Ultraviolet / Visible Absorption Spectra of MBT in Styrene and Pure Styrene

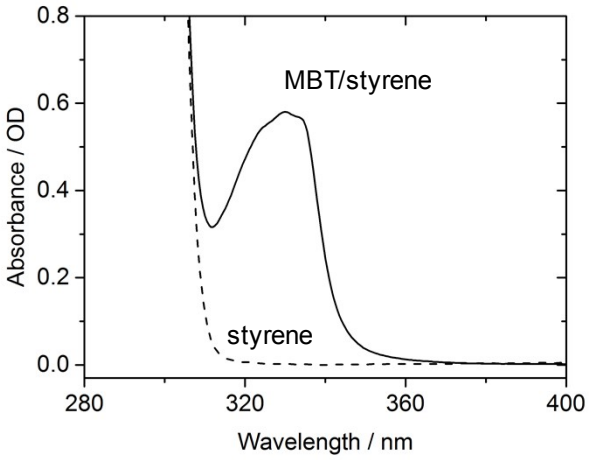

Figure S2: Steady state UV/vis absorption spectra of 0.56 mM MBT in styrene (solid line) and pure styrene (dashed line). The spectra were taken using a 380 μm pathlength sample.

4. Time-Resolved Electronic Absorption Spectroscopy of MBT in Toluene Solution

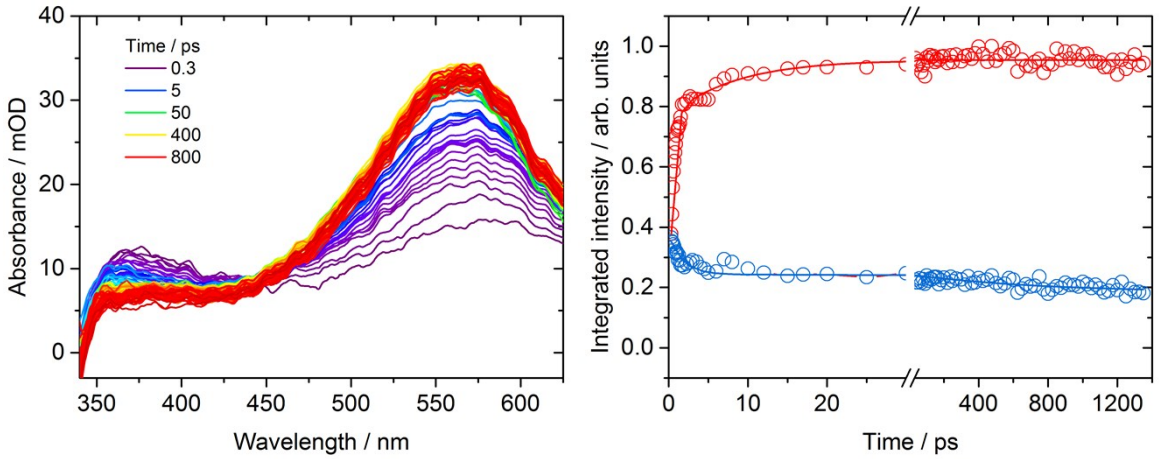

Figure S3: Transient electronic absorption spectra of 0.56 mM MBT in toluene solution following 330-nm excitation, and time-dependence of the intensities of the bands centered at 564 nm (red) and 370 nm (blue). TEA spectra of a pure toluene sample have been subtracted at each time delay to remove solvent interferences.

5. Spectral Decomposition of Time-Resolved Electronic Absorption Spectra of MBT in Methanol Solution

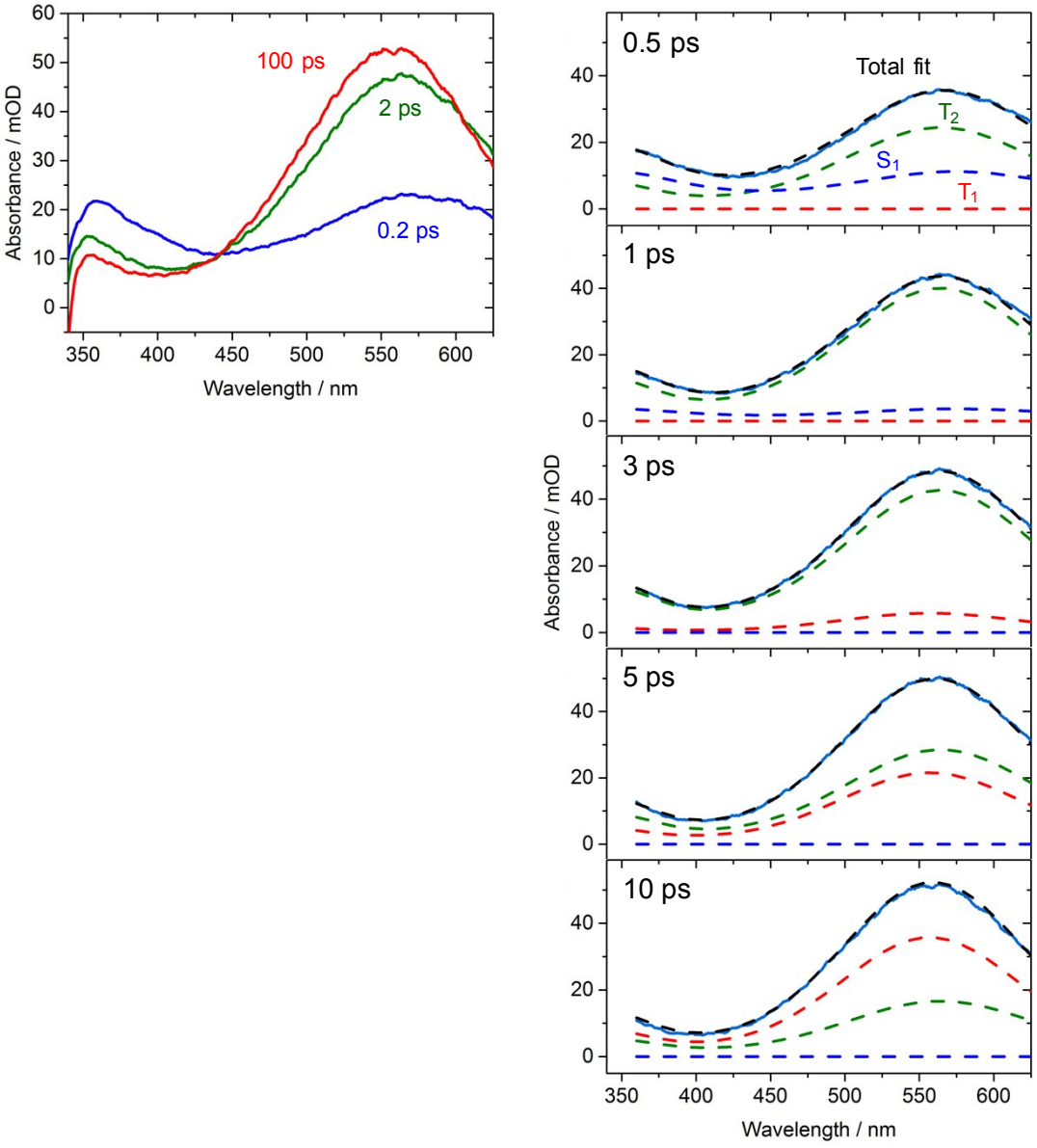

Figure S4: Left panel: TEA spectra of 0.56 mM MBT in methanol solution following 330-nm excitation at time delays of 0.2 (blue), 2.0 (green) and 100 ps (red). Right panel: examples of decomposition of TEA spectra for the MBT in methanol solution, with selected spectra obtained at time delays of 0.5, 1, 3, 5 and 10 ps. Blue: MBT S_1 absorption band, green: MBT T_2 band, red: MBT T_1 band, black: total fitting, light blue: the experimental spectrum at the indicated time delay. The spectral decomposition was carried out using the absorption spectrum at 0.2 ps for S_1 absorption, 2.0 ps for T_2 and 100 ps for T_1 (see the main text). This method assumes that each spectral shape did not change further with time.

6. Potential Energy Curves for MBT

Figure S5 shows computed optimized structures for excited states and MBT potential energy curves (PECs). The optimized S_1, T_1 and T_2 structures of MBT have several distinguishing features from the S_0 structure: all of the three excited state structures have longer C=S bond lengths (1.77, 1.78 and 1.80 Å for the S_1, T_1 and T_2 states) than the S_0 structure (1.64 Å) and the terminal S atom moves out of the molecular plane by 20-40°, which can be interpreted as pyramidalization at the carbon atom of the C=S bond. Moreover, the S_1 and T_1 structures show out-of-plane deformation at the N-H bond. Similarly distorted C=S structures have been reported previously for excited state geometries of other thione compounds.[10-12] For these reasons, the PECs are calculated along the C=S bond coordinate and as a function of the out-of-plane angles at the C=S and N-H bonds.

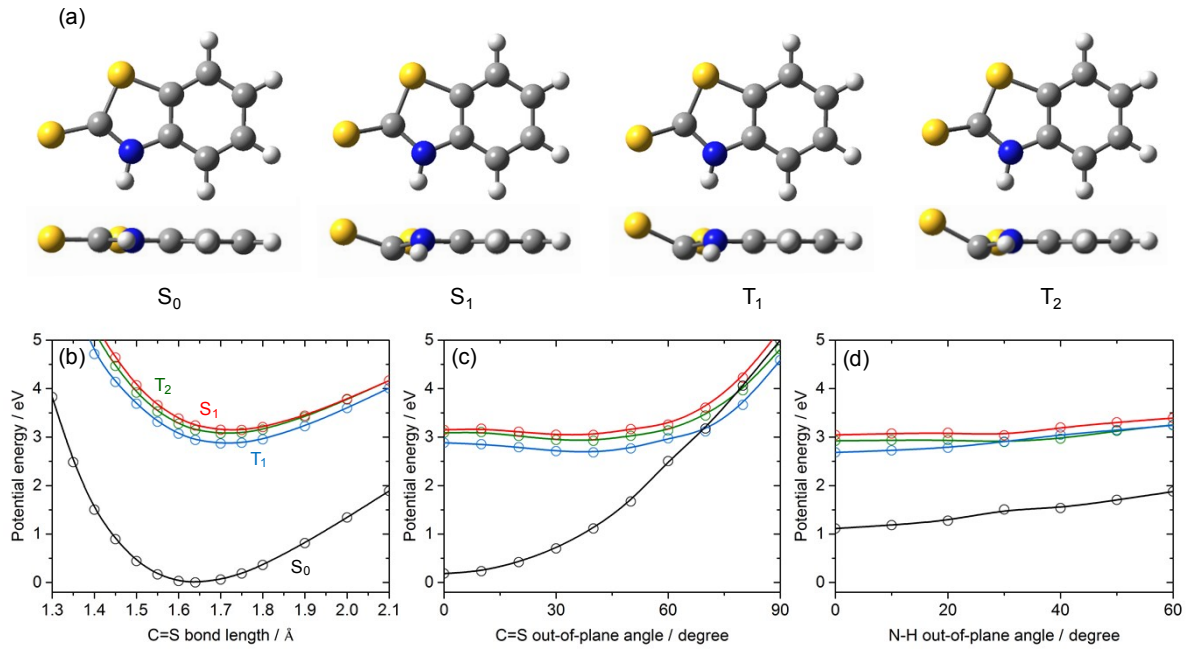

Figure S5: (a) Computed optimized structures for the S_0, S_1, T_1 and T_2 states of MBT at the CASPT2 (8/7)/cc-pVTZ level of theory, and representative potential energy curve cuts along (a) the C=S bond distance $R_{C=S}$; (b) the C=S bond out-of-plane angle $\varphi_{C=S}$ at $R_{C=S}$ = 1.75 Å; (c) the N-H bond out-of-plane angle φ_{N-H} at $R_{C=S}$ = 1.75 Å and $\varphi_{C=S}$ = 40°. The lowest two singlet (S_0; black, S_1; red) and triplet (T_1; blue, T_2; green) curves are shown.

The PECs show that the energy gap between the S_1 and T_2 states is ~0.1 eV or less over all of the computed degrees of freedom. This near degeneracy over wide regions of configuration space might promote ultrafast $S_1 \rightarrow T_2$ ISC. Internal conversion of other thione compounds (*e.g.*, 6-thioguanine and 2-thiouracil) from their S_2 to S_1 states is almost barrierless and ultrafast (less than 100 fs), according to both experiments and simulations.[11-14] If we assume that IC of MBT from the S_2 state to the S_1 state is also ultrafast and is complete within our instrument response time (~150 fs), the fastest components in the kinetic traces in Figure 2 can be attributed to $S_1 \rightarrow T_2$ ISC. Accordingly, we assign the slower component in the kinetic traces to IC from the T_2 state to the T_1 state.

7. Steady State FT-IR spectra of Styrene and of MBT in Styrene

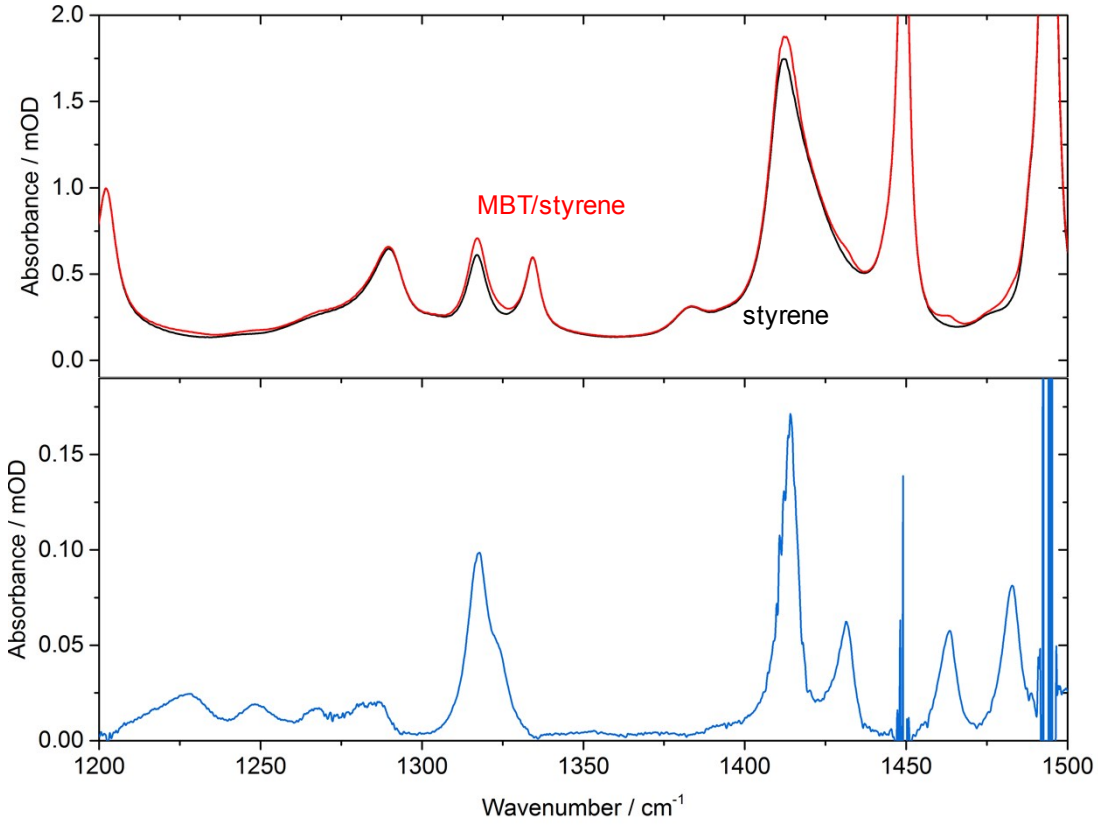

Figure S6: Upper panel: steady state FTIR spectra of styrene (black) and 24 mM MBT in styrene (red). Lower panel: difference spectrum obtained by taking the difference between spectra measured after and before adding MBT to the styrene. Each spectrum was obtained in a Harrick cell with a 50 μm thick spacer and CaF_2 windows.

8. Spectral Decomposition of Time-Resolved Vibrational Absorption Spectra of MBT in Toluene Solution

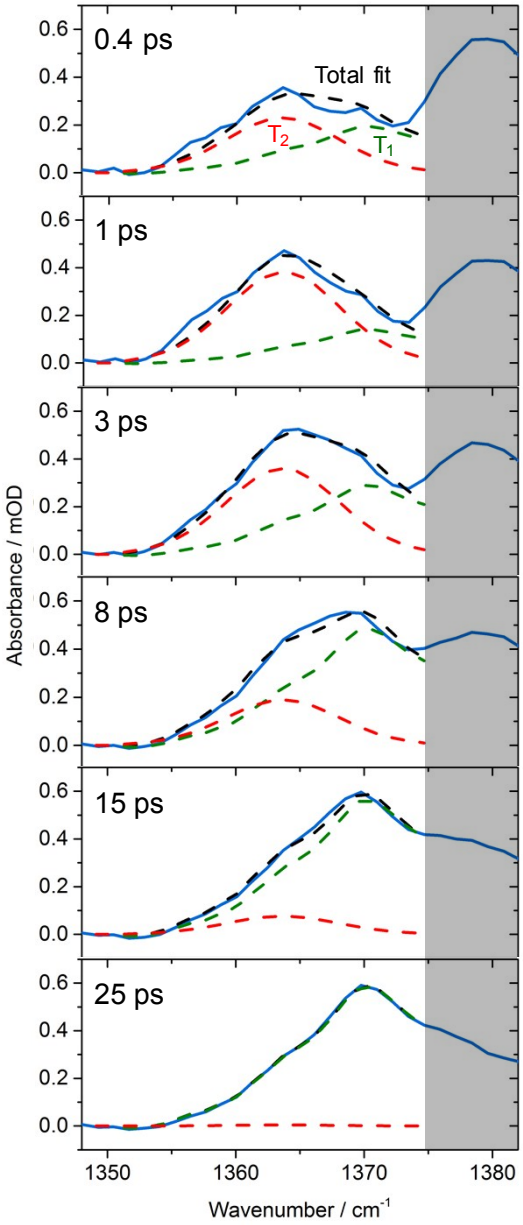

Figure S7: Example of decomposition of TVA spectra for 2.1 mM MBT in toluene solution following 330-nm excitation, with selected spectra obtained at time delays of 0.4, 1, 3, 8, 15 and 25 ps. Green: MBT T_1 absorption band at 1370 cm^{-1}, red: MBT T_2 band at 1364 cm^{-1}, black: total fitting, blue: the experimental spectrum at the indicated time delay. The spectral decompositions were restricted to the wavenumber region from 1350 cm^{-1} to 1375 cm^{-1} (see the main article). The spectral decomposition was carried out using the absorption spectrum at 50 ps for the T_1 band where vibrational cooling is expected to complete, and a Gaussian function with fixed band position and width for the T_2 band.

9. Computed Fundamental Infrared Transition Frequencies and Intensities for the MBT Excited States

Table S2: Calculated fundamental infrared frequencies and intensities of vibrational bands of the MBT S_1, T_1 and T_2 states, obtained at the CASPT2 (8/7)/cc-pVTZ and 6-311+G(d,p) levels of theory. The computed frequencies are shown over our experimental probe region (1240 - 1450 cm^{-1}). The infrared positions presented in the table are multiplied by a factor of 0.892 for the CASPT2 (8/7)/cc-pVTZ, and 0.881 for the CASPT2 (8/7)/6-311+G(d,p) results, so that the computed frequency for the T_1 band matches the observed T_1 band at 1370 cm^{-1}, which was assigned independently (see main text). Only calculated bands with band intensities greater than 10 km mol^{-1} are shown.

CASPT2 (8/7) / cc-pVTZ					
MBT S_1		MBT T_1		MBT T_2	
Frequency / cm^{-1}	Intensity / km mol^{-1}	Frequency / cm^{-1}	Intensity / km mol^{-1}	Frequency / cm^{-1}	Intensity / km mol^{-1}
1450	316	1430	46	1423	74
1434	50	1413	100	1384	70
1380	92	1370	108	1368	14
CASPT2 (8/7) / 6-311+G(d,p)					
MBT S_1		MBT T_1		MBT T_2	
Frequency / cm^{-1}	Intensity / km mol^{-1}	Frequency / cm^{-1}	Intensity / km mol^{-1}	Frequency / cm^{-1}	Intensity / km mol^{-1}
1446	204	1430	31	1424	61
1435	132	1406	63	1382	29
1384	112	1370	138	1363	103

10. Computed Vertical Excitation Wavelength, Oscillator Strength and Extinction Coefficient for the Triplet Biradical Addition Intermediate and the Lowest Triplet Excited State of Styrene

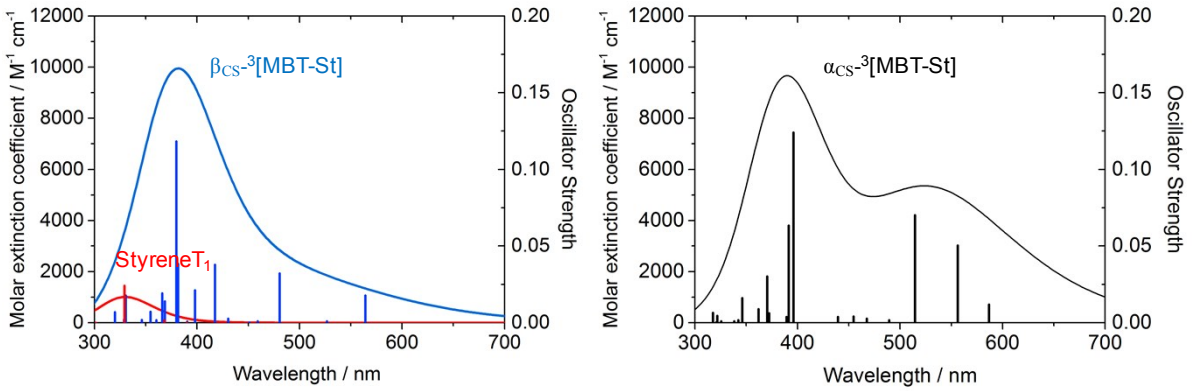

Figure S8: Computed oscillator strengths and simulated UV/vis absorption spectra obtained at the TD-DFT/6-311++G(3df,3pd) level of theory. Left panel: β_{CS}-^{3}[MBT-St] (blue) and ^{3}St (red), right panel: α_{CS}-^{3}[MBT-St].

11. Additional Information about the Reaction Pathway for the Lowest Excited Triplet State of MBT with Ground State Styrene

Our preferred assignment for the observed TVAS bands at 1264, 1307 and 1395 cm^{-1} is to the addition intermediate β_{CS}-^{3}[MBT-St], formed by the reaction of the thione sulfur atom at the β-position of styrene, as mentioned in the main article. Here, we consider the three other possible addition intermediates, for which chemical structures are provided below.

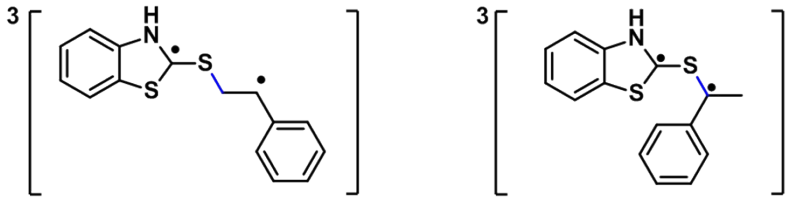

β_{CS}-^{3}[MBT-St] α_{CS}-^{3}[MBT-St]

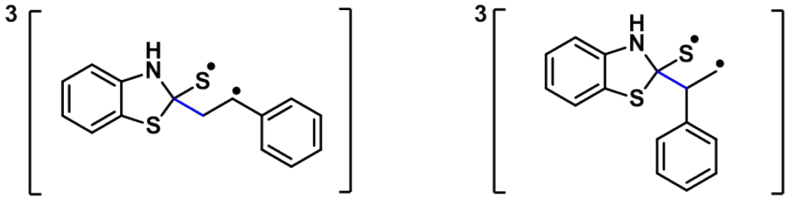

β_{CC}-^{3}[MBT-St] α_{CC}-^{3}[MBT-St]

The computed fundamental infrared band positions and intensities for α_{CS}-^{3}[MBT-St] in our observation window are essentially the same as for β_{CS}-^{3}[MBT-St] (Table S3), and agree with the experimentally observed band positions. However, our DFT calculations of the energetics of addition of T_1 MBT at the α- and β-positions of styrene, as illustrated in Figure S9, predict that the enthalpy of activation for the reaction at the α-position of styrene is 14.1 kJ/mol larger than the corresponding reaction at the β-position. Furthermore, the resulting biradical product α_{CS}-^{3}[MBT-St] is energetically unfavorable with respect to MBT (T_1) + Styrene (S_0) reactants.

The computed UV/vis absorption spectra for β_{CS}-^{3}[MBT-St] and α_{CS}-^{3}[MBT-St] shown in Figure S8 support these arguments: the computed spectral shape for α_{CS}-^{3}[MBT-St] is clearly

different from the extracted spectral shape for the addition product (Figure 5(c) in the main article).

The calculated fundamental infrared frequencies for α_{CC}-^{3}[MBT-St] and β_{CC}-^{3}[MBT-St] are slightly different from the experimentally observed band positions. In addition, the respective computed enthalpies of activation are 30.8 kJ/mol 18.4 kJ/mol higher than the reaction for β_{CS}-^{3}[MBT-St]. The computed enthalpy of activation for the reaction of the thione sulfur atom at the β-position of styrene (1.3 kJ/mol) is much lower than the three other candidates (15.4 - 32.1 kJ/mol), and is the only value consistent with the fast addition timescale (~100 ps). Consequently, we discounted the other three candidate structures for the adduct of MBT (T_1) with St (S_0) and assigned the three bands to β_{CS}-^{3}[MBT-St].

Table S3: Computed infrared positions and intensities for the candidate triplet state biradical adducts over our experimental probe region (1240 cm^{-1} - 1450 cm^{-1}). Calculations were performed at the B3LYP /6-311++G(3df,3pd) level of theory. The infrared positions presented in the table are corrected by a linear function described in the main text. Only calculated bands with band intensities greater than 5 km mol^{-1} are shown.

α_{CS}-^{3}[MBT-St]		β_{CC}-^{3}[MBT-St]		α_{CC}-^{3}[MBT-St]	
Frequency / cm^{-1}	Intensity / km mol^{-1}	Frequency / cm^{-1}	Intensity / km mol^{-1}	Frequency / cm^{-1}	Intensity / km mol^{-1}
1252	35	1257	11	1271	10
1262	21	1265	9	1305	52
1312	63	1304	52	1376	37
1389	68	1376	43	1405	13
1444	78	1447	55	1448	46

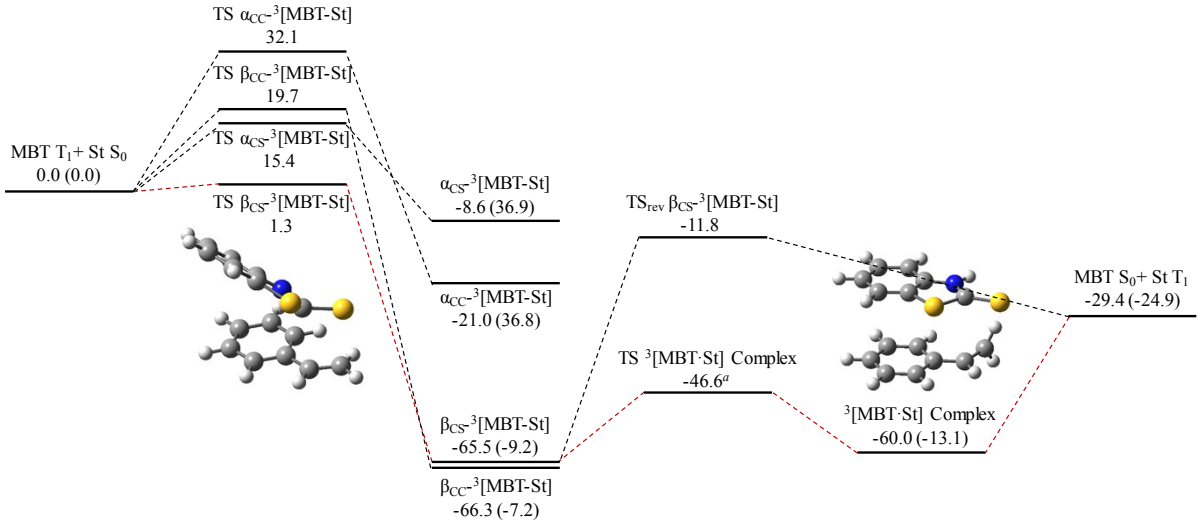

Figure S9: Schematic energy diagram for the addition reactions of MBT (T_1) at the α- and β-positions of styrene, obtained with the CAM-B3LYP-D3/6-311+G(d,p) level of theory. The values in the figure represent enthalpy changes, with Gibbs free energy changes in parentheses, relative to the sum of the energies of the MBT T_1 state and ground state styrene. Our preferred reaction pathway is highlighted in red. Representative optimized geometries are also shown. [a] The energy of the TS ^{3}[MBT·St] complex is an estimated value obtained from a relaxed potential energy scan.

The evidence from our TVA spectra indicates that the β_{CS}-^{3}[MBT-St] adduct dissociates to ground state MBT (S_0) and styrene (T_1) on timescale of ~650 ps, to complete the process of triplet quenching of the MBT (T_1). The activation energies presented in Figure S9 indicate that the direct dissociation pathway through the transition state labelled as TS_{rev} β_{CS}-^{3}[MBT-St] is unfavorable, because the enthalpy of activation for this dissociation pathway is 54.5 kJ/mol (if we assume that all the excess internal energy of the β_{CS}-^{3}[MBT-St] adduct has been quenched by the solvent bath), which is too high for the 650 ps timescale dissociation. The dissociation pathway can instead be understood if it proceeds *via* a complex state between MBT (S_0) and styrene (T_1) for which the optimized geometry is illustrated in Figure S9. The estimated energy barrier for this pathway is 18.9 kJ/mol. Computed infrared frequencies for the complex predict almost the same infrared band positions as for non-complexed MBT S_0

and styrene T_1products of the triplet quenching. Therefore, the observed disappearance of the β_{CS}-^{3}[MBT-St] bands and the apparent recovery of MBT S_0 band bleaches at 1318 cm^{-1} and 1414 cm^{-1} can be rationalized by this dissociation mechanism. The energy of the complex is higher than β_{CS}-^{3}[MBT-St], but inclusion of entropic effects (in the calculated Gibbs energies reported in Fig S9) shows that the formation of the complex state becomes favorable. Over an undetermined timescale, this complex will dissociate to MBT (S_0) and St (T_1), or perhaps ISC will relax the triplet character of the St component.

12. Time-Resolved Electronic and Vibrational Absorption Spectroscopy of Thioxanthone in Methanol and Styrene Solutions

We considered, and argued against triplet styrene contributions on the basis of evidence from TEA spectra (Section 3.2.1 in the main article) but also carried out further checks of the observed TVAS bands at 1264, 1307 and 1395 cm^{-1} using the triplet sensitizer, thioxanthone in place of MBT. Triplet energy transfer from thioxanthone to styrene has been reported previously.[15] The resulting TEA and TVA spectra are provided in Figure S10. If the observed TVAS bands are derived from triplet styrene, observation of the same bands is expected in experiments with thioxanthone. The TEAS features for thioxanthone in styrene solution decay completely within our experimental time range, suggesting a reaction or energy transfer is taken place with styrene. However, TVAS of thioxanthone in styrene demonstrates no product bands at 1264, 1307 and 1395 cm^{-1}, ruling out the assignment of such features to triplet styrene. The TVAS results do not discount completely the formation of triplet excited state styrene, because our DFT calculations suggest any triplet styrene bands are too weak to be observed (Table S4 for the calculated infrared positions and band intensities for triplet styrene), but do confirm that the features at 1264, 1307 and 1395 cm^{-1} belong to another intermediate species.

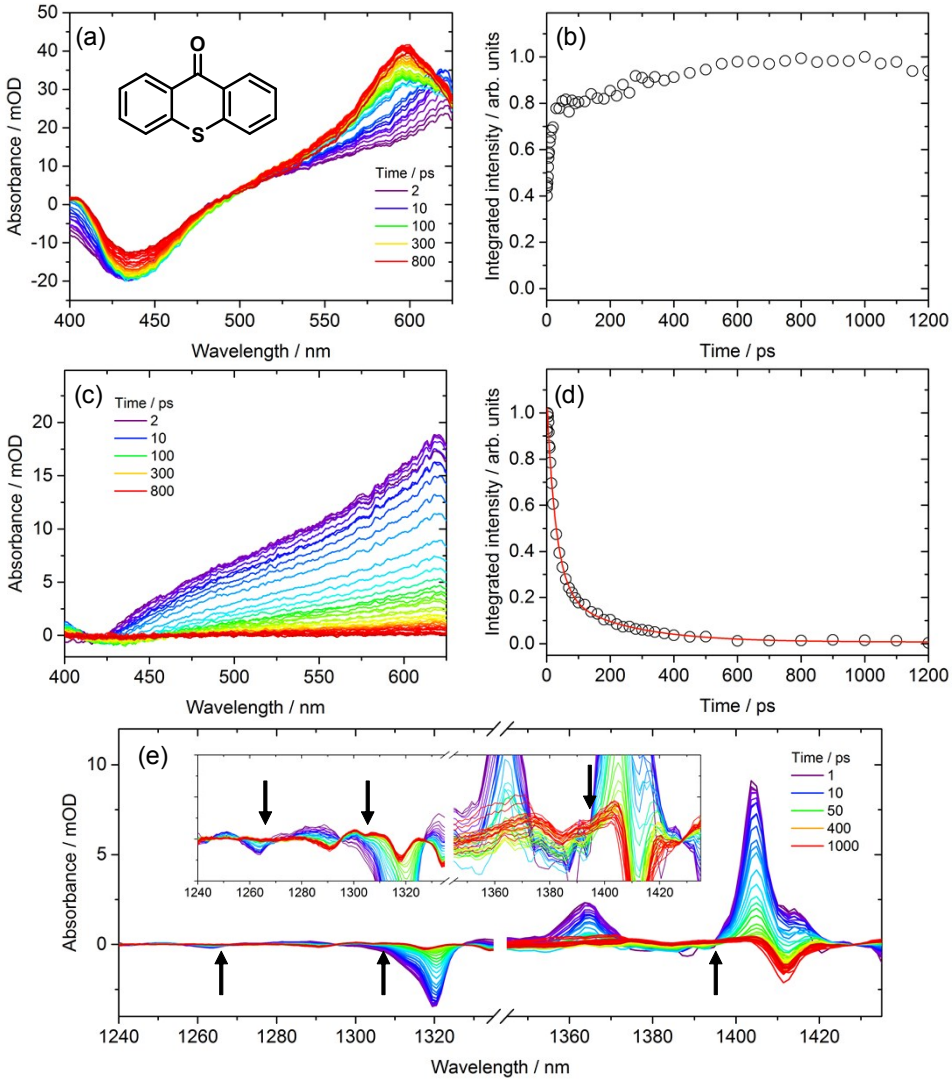

Figure S10: Transient absorption spectra of thioxanthone in methanol and styrene solutions following 370-nm excitation. Transient electronic spectra are shown for 2.4 mM thioxanthone in (a) methanol, and (c) styrene solution. The time-dependences of the band intensities at 598 nm are shown for (b) methanol and (d) styrene solution. The solid line in (d) represents biexponential fitting of the band intensity, giving time constants of τ_1 = 29 ± 3 ps and τ_2 = 209 ± 72 ps. The initial rise of absorption intensity on a timescale of ~30 ps observed in the methanol solution is not seen in the styrene solution, which is perhaps because the band peak at early times is out of our probe window. Panel (e) shows transient vibrational absorption spectra of 9.2 mM thioxanthone in styrene. The inset is an expanded view of the TVA spectra. The arrows correspond to the band positions mentioned in the main text (1264, 1307, 1395 cm^{-1}). Spectral overlap at around 1395 cm^{-1} prevents a definitive conclusion about the presence or absence of the band observed at this wavenumber for MBT in styrene, but it is evident that there are not positive bands at 1264 cm^{-1} and 1307 cm^{-1} (see the main article for further discussion).

Table S4: Calculated infrared band positions and intensities for the first triplet excited state of styrene over our experimental probe region (1240 cm^{-1} - 1450 cm^{-1}). Calculations used the Gaussian 09 package and the B3LYP functional with the 6-311++G(3df,3pd) basis set. The infrared band positions presented in the table are corrected by a linear function mentioned in the main text.

Frequency / cm^{-1}	Intensity / km mol^{-1}
1291	2
1316	1
1360	3
1400	4
1439	6

REFERENCES

1. M. J. Frisch, G. W. Trucks, H. B. Schlegel, G. E. Scuseria, M. A. Robb, J. R. Cheeseman, G. Scalmani, V. Barone, B. Mennucci, G. A. Petersson et al. *Gaussian 09, Revision B.01, Gaussian Inc., Wallingford CT*, 2009.
2. C. Lee, W. Yang and R. G. Parr, *Phys. Rev. B*, 1988, **37**, 785.
3. A. D. Becke, *J. Chem. Phys.*, 1993, **98**, 5648.
4. T. Yanai, D. P. Tew and N. C. Handy, *Chem. Phys. Lett.*, 2004, **393**, 51.
5. S. Grimme, J. Antony, S. Ehrlich and H. Krieg, *J. Chem. Phys.*, 2010, **132**, 154104.
6. N. Chéron, D. Jacquemin and P. Fleurat-Lessard, *Phys. Chem. Chem. Phys.*, 2012, **14**, 7170.
7. H.-J. Werner, P. J. Knowles, G. Knizia, F. R. Manby, M. Schütz, P. Celani, T. Korona, R. Lindh, A. Mitrushenkov, G. Rauhut et al. *MOLPRO, version 2010.1, A Package of Ab Initio Programs,* 2010.
8. T. H. J. Dunning, *J. Chem. Phys.*, 1989, **90**, 1007.
9. D. E. Woon and T. H. J. Dunning, *J. Chem. Phys.*, 1993, **98**, 1358.
10. L. Martínez-Fernández, L. González and I. Corral, *Chem. Commun.*, 2012, **48**, 2134.
11. L. Martínez-Fernández, I. Corral, G. Granucci and M. Persicob, *Chem. Sci.*, 2014, **5**, 1336.
12. S. Mai, P. Marquetand and L. González, *J. Phys. Chem. A*, 2015, **119**, 9524.
13. M. Pollum and C. E. Crespo-Hernández, *J. Chem. Phys.*, 2014, **140**, 071101.
14. S. Mai, P. Marquetand and L. González, *J. Phys. Chem. Lett.*, 2016, **7**, 1978.
15. R. Bonneau and B. Herran, *Laser Chem.*, 1984, **4**, 151.